Journal of Energy Storage 73 (2023) 108772

Contents lists available at ScienceDirect

Journal of Energy Storage

journal homepage: www.elsevier.com/locate/est

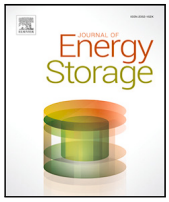

Research papers

A novel methodology to study and compare active energy-balance architectures with dynamic equalization for second-life battery applications

Roberto Di Rienzo *, Niccolò Nicodemo, Alessandro Verani, Federico Baronti, Roberto Roncella, Roberto Saletti

Dipartimento di Ingegneria dell'Informazione, University of Pisa, Via Caruso 16, Pisa, 56122, Italy

ARTICLE INFO

Keywords:
Second-life battery applications
Dynamic balancing approach
Active energy balance architectures
Battery Management System

ABSTRACT

The continuous growth of the electric vehicles market and the increasing environmental awareness impose to search for innovative solutions to reuse the exhausted vehicle batteries in different applications. One of the main problems of second-life batteries is the very high mismatch among their cell capacities which reduces the overall battery performance. The mismatch effect can be overcome by using dynamic equalization. This technique aims to keep balanced as much as possible the State of Charge of the cells during the battery operation, i.e. in both the charge and discharge phases. In order to do this, the dynamic equalization approach requires a high-current active energy balancing system able to move a quantity of charge among the battery cells much higher than the active balancing circuits sometimes used in first-life batteries. The use of a high equalization current increases the design complexity of the balance system.

A methodology to study and compare the main balance system topologies suitable for second-life batteries with dynamic equalization approach is presented in this work. The Adjacent Cell-to-Cell, Direct Cell-to-Cell, Cell-to-Pack, and Pack-to-Cell active balance topologies are analyzed considering the case study of a second-life battery composed of 10 series-connected cells with capacity values uniformly distributed around±15 % of the nominal value.

The investigation proves that the Direct Cell-to-Cell topology has the best performance. This balancing topology improves the usable battery capacity of around 16 % with respect to the case in which no dynamic equalization is applied if a DC/DC converter with a power efficiency of only 70 % is used. Finally, the results show that the Adjacent Cell-to-Cell performance is strongly affected by the position of the cell mismatches in the battery.

1. Introduction

The use of aged batteries in second-life applications is becoming more and more important thanks to the increased number of battery packs that reach the end of their first life in electric vehicles. Usually, the first life of the traction batteries ends when the remaining capacity reaches the 70–80 % of the brand-new capacity. Furthermore, the increasing concern about climate change and the need of a responsible use of the natural resources push toward the complete utilization of such remaining capacity, by reusing the aged batteries in applications where the requirements are less demanding [1]. Stationary applications are the most promising ones , where batteries are used to reduce the load peaks in the electricity distribution network and to mitigate the intermittent production of renewable energy sources [2,3]. Stationary applications often require batteries with high energy capabilities but less demanding in terms of power. In fact, these batteries are usually charged and discharged once a day with rather low current rates. For example, the batteries used as energy storage systems in the electricity distribution network are charged during the off-peak hours between 9 pm and 5 am and discharged in the remaining time [4].

As a general rule, the usable capacity of a battery composed of series-connected cells is limited by the capacity of the less performing cell [5]. Therefore, brand-new battery packs are manufactured with cells that show very limited capacity mismatch among them. In any case, charge equalization or balancing procedures are applied whenever a charge mismatch among the cells is detected. These procedures are usually applied at the end of a full charge and restore the fully balanced battery status. Charge equalization is one of the most studied issues of lithium-ion batteries. In recent years, many equalization circuits and algorithms were published in the literature and compared in many review studies [6–8]. These studies usually divide the equalization

* Corresponding author.
E-mail address: roberto.dirienzo@unipi.it (R. Di Rienzo).

https://doi.org/10.1016/j.est.2023.108772
Received 3 April 2023; Received in revised form 11 August 2023; Accepted 17 August 2023
Available online 31 August 2023

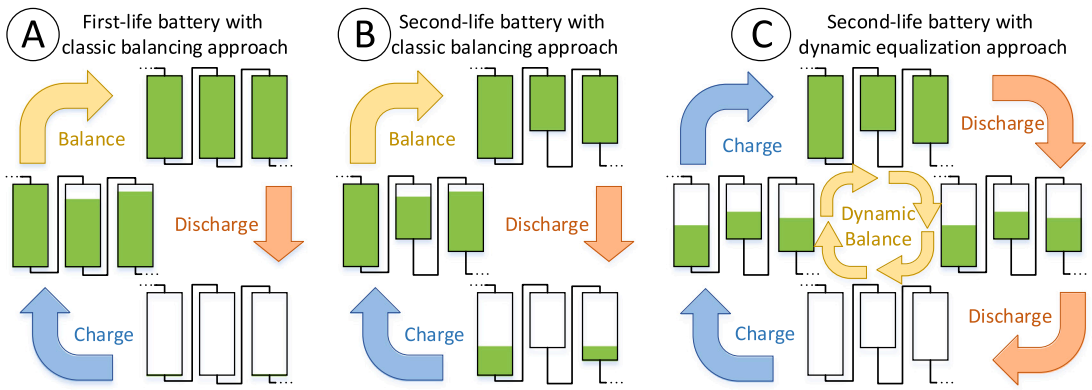

Fig. 1. Comparison between the classic balancing approach applied to the first and second-life batteries, and the dynamic equalization approach applied to second-life batteries.

approaches in two groups: passive and active. The passive approach consists of using one or more bleeding resistors to discharge the most charged cells to a level corresponding to the lowest charged one. The result is that the stored charge is equalized in each of the series-connected cells of the battery [9] and the extra charge is wasted on purpose. Instead, the active approaches aim to move the stored charge from the most charged cells to the most discharged ones thus reducing the amount of wasted energy. Passive techniques are the most used in first-life batteries, in which the fresh cells present very uniform capacity and self-discharge current values [10]. Thus, the small amount of energy recovered by the active techniques does not justify the higher cost of the balancing circuit [9].

While brand-new batteries show a very uniform distribution of the individual cell capacities, second-life batteries are instead characterized by a larger variability of the cell capacities, which gradually increases with the battery aging [10]. This fact leads to the problem that the charge potentially available in the battery cannot fully be used, even if the battery cells are balanced at the end of the charging stage. In fact, the discharge process is interrupted when the weakest cell reaches its cut-off voltage, while residual charge is still available in the other cells. This problem can be overcome by using the dynamic equalization technique [11], which uses an active charge equalization system to move charges from the cells with higher capacity to the cells with lower capacity while the battery is in use [12,13].

It is important to note that the goal of dynamic equalization is completely different from that of active balancing. In fact, the active balancing process aims to equalize the charges stored in the cells in some specific moments of the battery life, for example at the end of the charge. Instead, the dynamic equalization procedure aims to continuously keep the state of charge of each cell of the battery equal as much as possible to the others, during both the charge and discharge phases. In this way, all the battery cells can fully be charged and discharged, thus maximizing the usable capacity of the battery, even if the capacities of its cells are widely spread [14].

Let us further discuss the difference between active charge balancing and dynamic equalization. The balancing technique applied to a first-life battery is shown in Fig. 1(A). As we can note, the very low charge mismatch among the cells can be balanced in the last part of the charging phase allowing the complete charge and discharge of the battery. On the contrary, second-life batteries contain aged cells whose capacity and self-discharge current can show an important mismatch, even larger than 15 % [15]. This value makes passive balancing systems and low-current active ones not suitable for second-life batteries, as shown in Fig. 1(B). Second-life batteries instead require a Battery Management System (BMS) equipped with a high-current active balancing circuit that performs a dynamic equalization approach as shown in Fig. 1(C) [16,17]. The dynamic equalization must always be active for the entire duration of the charge and discharge phases, to maintain the State of Charge of all the battery cells balanced, and to allow the complete exploitation of the charge stored in the battery.

Dynamic equalization requires a high equalization current to allow a large quantity of charge to be exchanged. These specifications make the choice of the most suitable active equalization topology difficult. Many literature works compare the Adjacent Cell-to-Cell (AC2C), Direct Cell-to-Cell (DC2C), Cell-to-Pack (C2P), and Pack-to-Cell (P2C) active balancing architectures using both theoretical and simulative approaches for the first-life applications [18–25]. For example, Qu et al. in [18] show that the DC2C architectures have the best performance but require complex hardware structures and control algorithms. Moreover, C2P and P2C can be good alternatives to DC2C for small-size batteries. However, these works merely analyze the case in which the battery is composed of new cells with very low variability of the parameters, in which the active balancing process is only used. To the best of our knowledge, active equalization topologies have never been compared in second-life case studies to implement the dynamic equalization approach.

The aim of this work is to overcome this research gap, to study and compare the main active equalization topologies, and to help the designer in the choice of the best architecture for second-life BMS design. The Adjacent Cell-to-Cell, Direct Cell-to-Cell, Cell-to-Pack, and Pack-to-Cell equalization topologies are modeled using a theoretical approach and applied to a second-life battery case study. We used a simulative platform developed in Matlab Simulink to investigate the dynamic equalization topologies. The simulative approach was preferred to avoid the complexities of the physical realization of the equalization systems investigated and to obtain results as much general as possible in terms of balancing circuits and mismatches of the cell capacities. However, the results obtained by simulation can easily be extended to real physical implementations, by using the experimental data from literature works on the active balancing topologies, as it will be shown in Section 7.

The rest of the paper is organized as follows: Section 2 reports on the methodology applied to study the main active balancing topologies for the dynamic equalization approach in second-life applications. A brief description and the results obtained for the AC2C, DC2C, C2P, and P2C topologies are reported in Sections 3, 4, 5, and 6, respectively. Section 7 analyzes, discusses the results, and compares the studied topologies. Finally, the main work conclusions are summarized in the last section.

2. Methodology

Large battery packs are usually composed of modules connected in series and/or parallel. Each module is in its turn consists of elementary cells, and it is usually equipped with a dedicated electronic system that includes the equalization circuit. For the sake of simplicity, this work focuses on the dynamic equalization inside the module, but the same concepts could easily be applied to the equalization of the capacity

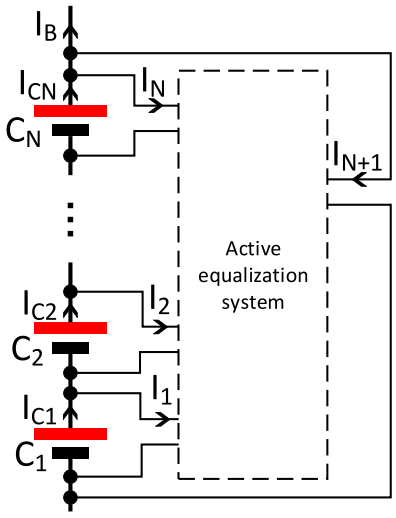

Fig. 2. Block diagram of generic active equalization system applied to a battery composed of N series-connected cells.

mismatch among the modules of the battery pack. As such, the terms battery, battery pack, and module are used without distinction and refer to one battery module.

The generic block diagram of an active equalization system applied to a battery composed of N series-connected cells is reported in Fig. 2 [22]. It consists of an $N+1$-port system able to move energy from one port to another one. The path of the energy flux can be used to classify the active equalization techniques in Adjacent Cell-to-Cell, Direct Cell-to-Cell, Cell-to-Pack, and Pack-to-Cell topologies [8,18]. The AC2C topology uses the N ports connected to the cells to move energy from any cell to its adjacent ones only. The DC2C techniques, instead, are able to move energy from any cell of the pack to any other. Both these techniques do not use the port labeled $N+1$ that is instead used in the P2C and C2P techniques. The port $N+1$ is connected to the terminals of the battery pack and allows the P2C and C2P architectures to move energy from the entire pack to a single cell and vice versa, respectively.

Each energy transfer is characterized by an efficiency value that depends on the equalization circuit utilized. The equalization circuit can be represented by one or more DC/DC converters that are connected to the input and output ports of the equalization system by means of a switch matrix. To keep the following discussion as general as possible, the details of the specific equalization circuits are neglected, and the process of energy transfer from port i to port o is modeled as:

$$P_o = \mu P_i \tag{1}$$

where P_o is the output power at port o, P_i is the input power at port i, and μ is the power efficiency of that particular energy transfer. Po and P_i are the product of the voltage and current at the corresponding converter port. The voltage at converter ports $1 \ldots N$ is the same of the corresponding cell voltage, while the voltage at port $N+1$ is equal to the battery voltage (*i.e.*, the sum of all the cell voltages). The cell voltage is the contribution of the open circuit voltage, which mainly depends on the cell state of charge (SoC), and a dynamic term that depends on the cell current through its impedance [26].

The dynamic equalization technique aims at leveling the SoC of each battery cell at any time during the battery operation, by varying the cell current according to its actual capacity. Thus, we can assume that the battery cells have a very similar SoC when dynamic equalization is active. This in turn implies that all the cells have a very similar open circuit voltage. Thus, cell voltages can differ only for the dynamic term. However, the dynamic term is usually small compared to the open circuit voltage [27], thus its variation among the battery cell, due to cell impedance mismatch, can safely be neglected. In conclusion, the cell voltages are assumed to be uniform in the battery for the purpose of this work. In fact, as shown above, this is a good approximation when dynamic active equalization is applied and avoids the complications of using a dynamic cell model to compute its voltage. This allows Eq. (1) to be written only in terms of the input and output port currents, I_i and I_o respectively, as:

$$\begin{cases} \mu = \frac{P_o}{P_i} = \frac{-I_o}{I_i} & \forall o, i = 1, \ldots, N \\ \mu = \frac{P_o}{P_i} = \frac{-N I_o}{I_i} & \forall i = 1, \ldots, N; o = N+1 \\ \mu = \frac{P_o}{P_i} = \frac{-I_o}{N I_i} & i = N+1; \forall o = 1, \ldots, N \end{cases} \tag{2}$$

where the first equation holds for AC2C and DC2C while the last two equations for C2P and P2C topologies, respectively.

It is now useful to recall the definition of SoC in the following equation:

$$SoC(t) \overset{\text{def}}{=} \frac{Q_C(t)}{C_C} = \frac{Q_C(t_i) - \int_{t_i}^{t} i(\tau) d\tau}{C_C} \tag{3}$$

where $Q_C(t)$ is the charge stored in the cell, C_C is the actual cell capacity and $i(\tau)$ is the cell current. The cell coulombic efficiency is neglected in (3) since it is very close to 1 for lithium-ion cells.

Starting from the definition of SoC in Eq. (3), we can calculate the charge (Q_j) that the dynamic equalization algorithm should move from/to the jth cell to reach the fully charged or discharged status at the end of the charge and discharge phases, respectively. For example, Eq. (4) shows the jth cell SoC when the cell is completely discharged at time t_f ($SoC_j(t_f) = 0$), starting from a fully charged condition at time t_i ($SoC_j(t_i) = 1$).

$$SoC_j(t_f) = \frac{C_{C_j} - \int_{t_i}^{t_f} (I_B + I_{N+1} + I_j) d\tau}{C_{C_j}} = 0 \tag{4}$$

The integral in (4) can be expressed as the sum of the three quantities of charge: Q_B, Q_{N+1}, and Q_j. Q_B is the charge provided by the battery to the external load and is therefore the exploited battery capacity C_B. Q_{N+1} and Q_j are the charges moved through the ports $N+1$ and j, respectively. The calculation of these charge quantities can be obtained in a closed form only if the power efficiency μ of the active equalization system is equal to 1 (ideal case) and 0 (passive balancing). In the ideal case, the charge balance in the equalization circuit is expressed by (5) as:

$$\sum_{j=1}^{N} Q_j + N Q_{N+1} = 0 \tag{5}$$

Moreover, Q_j can be written as $Q_j = C_{C_j} - Q_B - Q_{N+1}$ from (4) and therefore battery capacity C_B in the ideal case is:

$$C_B\Big|_{\mu=1} = \frac{\sum_{j=1}^{N} C_{C_j}}{N} \tag{6}$$

This equation states that the maximum usable capacity of the battery is equal to the average of the cell capacity values, independently of is the equalization topology used if its power efficiency is equal to one. The same result is obtained considering the opposite case in which the battery starts from a fully discharged condition and is fully charged. On the other hand, all the moved energy is wasted if μ is equal to 0, and so the battery capacity is equal to the minimum cell capacity.

$$C_B\Big|_{\mu=0} = \min_{j \in [1, \ldots, N]} C_{C_j} \tag{7}$$

Instead, the equalization topology affects the value of C_B if μ is different from 0 and 1 as it will be demonstrated in the next sections. The AC2C, DC2C, P2C, and C2P topologies are modeled and then applied to a simple case study (Case A) to analyze and compare the behavior of each one. Case A is a second-life battery composed of 10

cells with a capacity uniformly distributed in the range 20 A h ± 15 %, i.e., from 17 to 23 A h with steps of 0.66 A h. The cells are supposed to be arranged with increasing capacity from Cell 1 to Cell 10, with no loss of generality. Different cell arrangements will be considered and discussed if needed. Moreover, the accuracy of the cell SoC estimation is key to obtain a good dynamic equalization algorithm and to accurately control the battery behavior. Several improvements in the accuracy of the battery state estimation algorithms can be found in the literature [27,28]. Therefore, another assumption of this work is to consider the state estimation algorithm accurate enough to consider the capacity of each battery cell and its SoC known.

3. Adjacent Cell-to-Cell (AC2C)

The Adjacent Cell-to-Cell technique uses $N-1$ bidirectional DC/DC converters to move energy from any cell to one of two adjacent cells [18]. Its block diagram is shown in Fig. 3. It is derived from the diagram of Fig. 2 where the $N+1$th port is omitted and the charge transfer is only limited to adjacent cells. Flyback [21], Buck–Boost [29], and switched–capacitor [30] converters are the most frequently used circuits to realize these DC/DC converters. The flyback converter is more expensive because it requires a transformer, but its control algorithm is simpler than the other ones. On the other hand, the Buck–Boost converter is composed of a simple and cheap circuit but the control algorithm is more complex. The circuit of the switched–capacitor architecture is very simple and extremely cheap, being composed of capacitors that are connected alternatively between two adjacent cells. The drawback of this approach is the rather low balancing current.

Let us describe the equations derived from the application of this charge balance approach after a complete discharge phase according to the procedure described in Section 2.

$$\begin{cases} C_{C_1} = Q_B + Q_{1\,2} \\ C_{C_j} = Q_B - Q_{j\,j-1} + Q_{j\,j+1} \quad \forall j = 2, \dots, N-1 \\ C_{C_N} = Q_B - Q_{N\,N-1} \end{cases} \tag{8}$$

$$\begin{cases} Q_{j+1\,j} = \mu Q_{j\,j+1} & \text{if } Q_{j\,j+1} \geq 0 \text{ (when } j\,j+1 \text{ is the input port)} \\ Q_{j+1\,j} = \frac{1}{\mu} Q_{j\,j+1} & \text{if } Q_{j\,j+1} < 0 \text{ (when } j\,j+1 \text{ is the output port)} \end{cases} \tag{9}$$

To the best of our knowledge, the battery exploitable capacity C_B cannot be calculated in closed form using the AC2C model when μ is different from 0 or 1. The value of C_B depends on both the capacities and positions of the cells in the battery. However, an iterative procedure can be applied to obtain the quantities of charge to move among the cells to maximize the usable capacity of the battery and thus determining C_B. The procedure starts defining a target value (Q_{targ}) for Q_B and calculates the quantity of charge that must be moved from/to each cell to obtain this capacity value. $Q_{1\,2}$ is calculated according to the first equation of system (8) by substituting Q_{targ} to Q_B. Then, the second equation of system (8) and the system (9) are used to calculate $Q_{j\,j+1}$ for all battery cells with j index from 2 to $N-1$. Finally, the equation related to cell N provides a feedback on the Q_{targ} value chosen at the beginning of the iteration, as reported in (10).

$$\begin{cases} C_{C_N} + Q_{N\,N-1} > Q_{targ} \implies C_B > Q_{targ} \\ C_{C_N} + Q_{N\,N-1} = Q_{targ} \implies C_B = Q_{targ} \\ C_{C_N} + Q_{N\,N-1} < Q_{targ} \implies C_B < Q_{targ} \end{cases} \tag{10}$$

In particular, the sum of C_{C_N} with the charge quantity moved from cell $N-1$ to cell N ($Q_{N\,N-1}$) is the maximum charge that can be delivered from cell N. If this value is higher than Q_{targ}, there still remains some charge stored in cell N that is not delivered to the load, since the discharge ends due to the undercharge condition of the other cells. Therefore, C_B is higher than the current Q_{targ} value. Instead, if the sum $C_{C_N} + Q_{N\,N-1}$ is lower than Q_{targ}, the maximum charge that

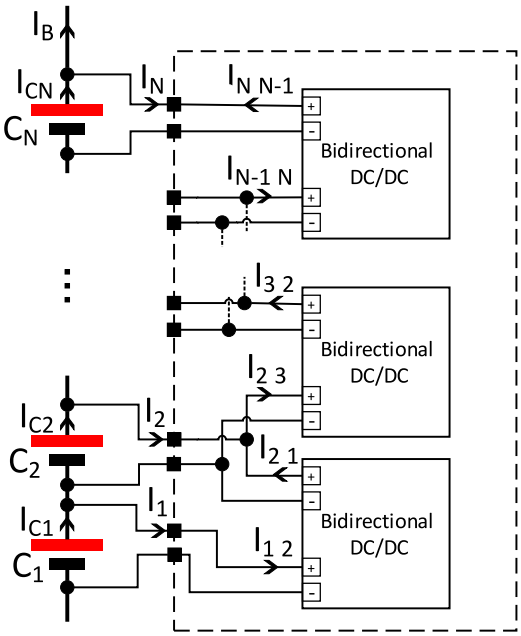

Fig. 3. Block diagram of a generic Adjacent Cell-to-Cell active equalization system applied to a battery composed of N series-connected cells.

can be extracted from the Nth cell, and thus from the battery, is lower than Q_{targ}. For these reasons, we find the value of Q_{targ} equal to C_B only when the available charge from Cell N is equal to Q_{targ}. Fig. 4 reports the $C_{C_N} + Q_{N\,N-1}$ as a function of Q_{targ} charge for different μ values obtained with the application of the described procedure to Case A. Q_{targ} is changed in a range from $C_B\big|_{\mu=0}$ to $C_B\big|_{\mu=1}$, i.e., the minimum (17 A h) and the average (20 A h) cell capacity in Case A.

The deliverable charge $C_{C_N} + Q_{N\,N-1}$ is equal to Q_{targ} for 17 A h and 20 A h with μ of 0 and 1, respectively, as theoretically demonstrated in (7) and (6). The dashed line identifies the optimal value C_B as a function of μ. The results show that the maximum charge extracted from the battery when dynamic equalization is applied decreases with the efficiency of the converter, as expected. Another interesting aspect highlighted by the results shown in Fig. 4 is the sensitivity of the dynamic equalization algorithm in calculating the equalization charges $Q_{j\,j+1}$. Choosing the proper values of the equalization charges $Q_{j\,j+1}$, and thus of the equalization times, is more difficult in equalization systems with low efficiency. In fact, the high slope of the low-efficiency curves may result in a large variation in the charge available in cell N (given by $C_{C_N} + Q_{N\,N-1}$) and so in C_B for a small error in setting the Q_{targ} value.

The maximum exploitable battery capacity C_B was obtained by comparing $C_{C_N} + Q_{N\,N-1}$ with Q_{targ}. The values reported in Fig. 4 (dashed blue line) for different values of μ depend on the initial hypothesis of cells order in ascending order of capacity. In fact, it should be noted that the C_B values obtained with the AC2C topology are strongly influenced by the distribution of the capacity mismatch among the cells of the battery. The arrangement of cells, ordered from the lowest to the highest capacity, forces the charge movement from the highest cells to the lowest ones, passing through all the intermediate cells. For each cell involved in the transfer, the starting quantity of charge is reduced because of the efficiency of the DC/DC converter. The net result is the lowest value of C_B. Indeed, Case A represents the worst distribution of mismatch, because it moves the largest quantity of charges before equalization is reached The procedure to calculate the maximum battery capacity C_B was repeated for all the possible permutations (10! = 3,628,800) of the battery cell position. The minimum,

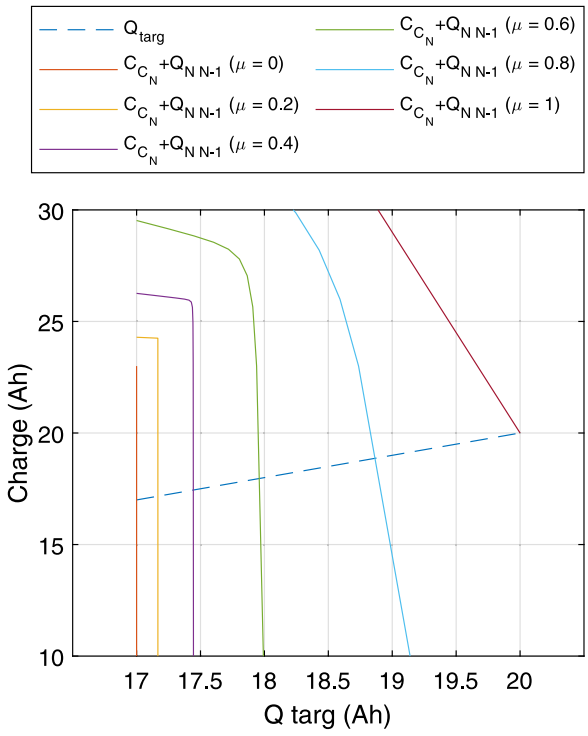

Fig. 4. Comparison between $C_{C_N}+Q_{N\,N-1}$ and Q_{targ} charges for different μ values. This comparison produces feedback to identify the battery capacity (C_B) using Eq. (10). (For interpretation of the references to color in this figure legend, the reader is referred to the web version of this article.)

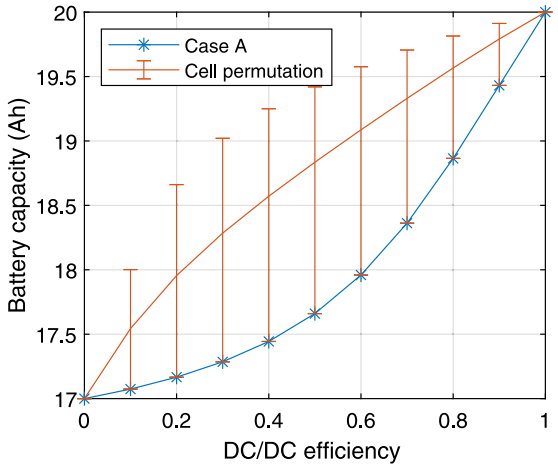

Fig. 5. C_B values obtainable with the Adjacent Cell-to-Cell topology for different DC/DC efficiency μ with the cell capacity distribution of Case A (blue line). The orange line shows the minimum, mean and maximum C_B values obtained by permuting the cell position of Case A. (For interpretation of the references to color in this figure legend, the reader is referred to the web version of this article.)

maximum, and mean (orange line) values of C_B for each μ are reported in Fig. 5.

As anticipated above, the arrangements of the cells from the lowest to the highest capacity and vice-versa are the worst conditions, because the largest quantity of charge is moved from the upper cells to the lower ones through the intermediate cells (and vice versa with the opposite order of the cells) before the equalization is reached. The best cell position arrangement is not the same for all the values of μ because μ influences the remaining quantities of charge in each step. Indeed, C_B is maximized by minimizing the number of charge movements. Cells

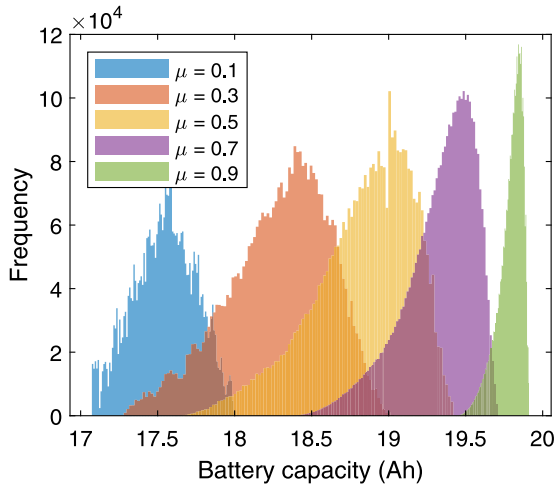

Fig. 6. Maximum battery capacity distribution for different μ obtained with all the possible permutations of the cell position starting from Case A.

with capacity mismatches of opposite signs with respect to the mean value should be placed the closest possible, to minimize the number of charge movements. The distributions of the maximum battery capacity C_B for all the cell permutations with μ of 0.1, 0.3, 0.5, 0.7, and 0.9 are reported in Fig. 6. It shows that C_B is strongly dependent on the cell arrangement. For example, it varies from 18.4 A h to 19.7 A h when μ is 0.7.

4. Direct Cell-to-Cell (DC2C)

The DC2C topologies aim to directly move energy from any cell of the battery to another one [18]. Fig. 7 shows the two main architectures used to implement the DC2C topology.

Each cell is equipped with one bidirectional isolated DC/DC converter with two ports in the first architecture (DC2Cp) [31]. One port is connected to the cell, while the second one is connected to a common bus. In this way, each converter moves energy from its cell to the bus and vice-versa, thus realizing a two-step transfer through two converters. The second DC2C architecture (DC2Cs) is composed of only one isolated DC/DC converter with one input and one output port [32]. The input and output ports can be connected to any cell of the battery through a switching network that must carefully be controlled to avoid short circuits between cells. The same model is used to describe the two architectures. It is reported in the following equation system:

$$\begin{cases} I_{C_j} = I_B + I_j \quad \forall j = 1, \dots, N \\ -\sum I_o = \mu \sum I_i \end{cases} \tag{11}$$

where o and i are the indices of the cells that are charged and discharged, respectively. The parameter μ has a different meaning for the two architectures. It is the product of the energy efficiencies of the bidirectional DC/DC converters used to move energy from cell i to the bus and from the bus to cell o in the DC2Cp architecture. Instead, μ is the product of the efficiencies of the switching network and the unidirectional DC/DC converter in the DC2Cs architecture. The current equations reported in system (11) can be transformed in charge equations using the same approach applied to the AC2C topologies. Also in this case, C_B cannot be derived with a closed-form equation, but it can easily be obtained with an iterative procedure. The process starts defining a value of Q_{targ} and calculating the quantity of charge to be moved from/to each cell replacing Q_{targ} to Q_B in the first equation of (11) that is written as:

$$Q_j = C_{C_j} - Q_{targ} \quad \forall j = 1, \dots, N \tag{12}$$

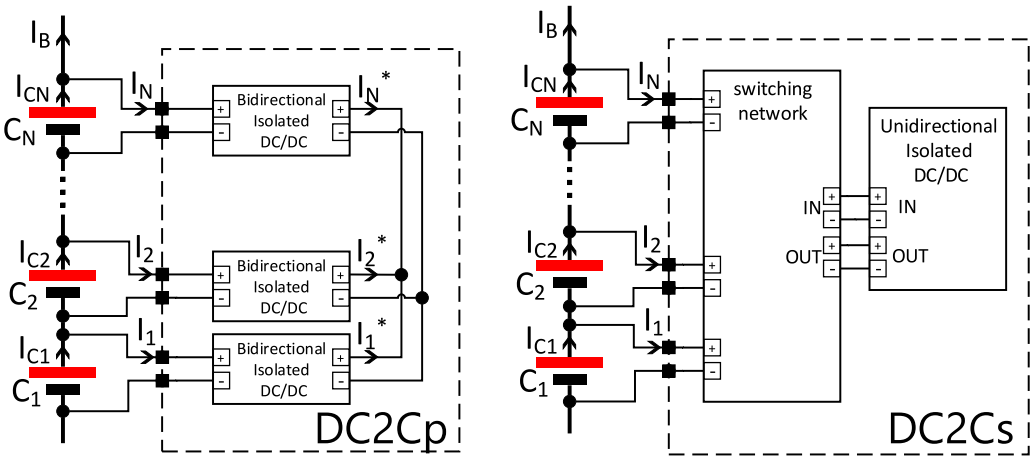

Fig. 7. Block diagram of the two main topologies of Direct Cell-to-Cell active equalization system applied to a battery composed of N series-connected cells.

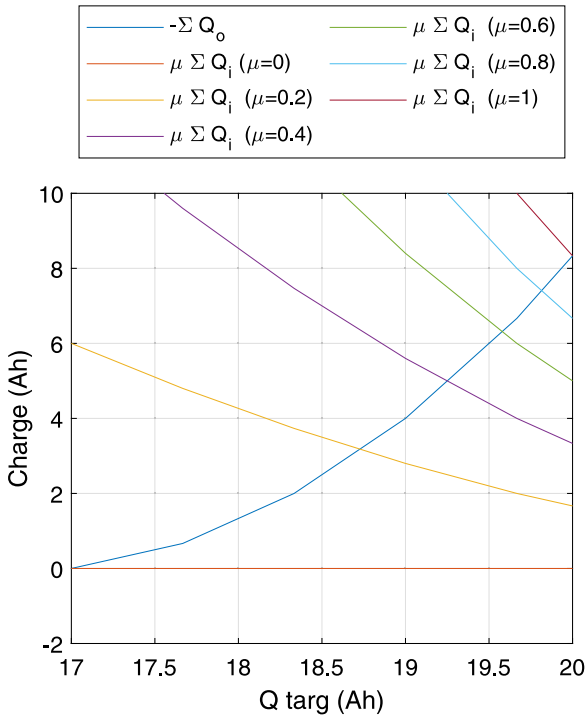

Fig. 8. Comparison between $-\sum Q_o$ and $\mu \sum Q_i$ charges for different μ values. This comparison produces a feedback to identify the battery capacity using the equation system (13).

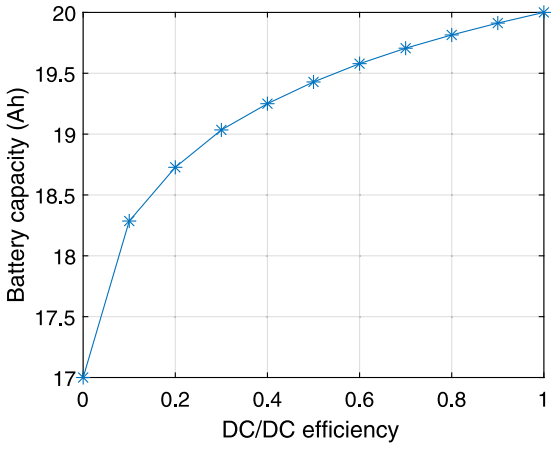

Fig. 9. C_B values obtainable with the Direct Cell-to-Cell topology for different DC/DC efficiency μ with the cell capacity distribution of Case A.

The feedback on the Q_{targ} value is produced by the second equation of the system (11) which is rewritten with the charge variables. The feedback effect at the end of the iteration is reported in the equation system (13).

$$\begin{cases} -\sum Q_o < \mu \sum Q_i \implies C_B < Q_{targ} \\ -\sum Q_o = \mu \sum Q_i \implies C_B = Q_{targ} \\ -\sum Q_o > \mu \sum Q_i \implies C_B > Q_{targ} \end{cases} \tag{13}$$

The procedure is applied to Case A varying Q_{targ} in the range from $C_B\big|_{\mu=0}$ to $C_B\big|_{\mu=1}$ and μ from 0 to 1. Fig. 8 reports the diagrams of $-\sum Q_o$ and $\mu \sum Q_i$ for several values of μ, whereas Fig. 9 summarizes the battery capacity values obtainable as a function of the DC/DC converter transfer efficiency. C_B ranges from 17 A h to 20 A h, as expected for $\mu = 0$ and $\mu = 1$.

5. Pack-to-Cell (P2C)

The energy moves from the entire battery pack to a single cell in the P2C topologies. Two different P2C architectures can be identified. Their block diagrams are shown in Fig. 10. The first architecture (P2Cs) consists of a unidirectional DC/DC converter with the input port connected to the battery pack and the output port connected to a switch matrix that selects one particular battery cell [33,34]. Instead, the second architecture (P2Cp) consists of a unidirectional DC/DC converter with the input port connected to the battery pack and N output ports, one for each cell composing the battery pack [35].

The two P2C architectures can be described by the same equation system using the approach applied to the DC2Cp and DC2Cs architectures. The P2C equation system is reported in (14) and is obtained by applying the Kirchhoff's law to each cell and imposing the correct sign of the current value to each DC/DC port, together with the efficiency equation of the energy transfer, i.e. Eq. (1).

$$\begin{cases} I_{C_j} = I_B + I_{N+1} + I_j \quad \forall j = 1, \dots, N \\ I_j \le 0 \quad \forall j = 1, \dots, N \\ I_{N+1} \ge 0 \\ -\sum_{j=1}^{N} I_j = \mu N I_{N+1} \end{cases} \tag{14}$$

An iterative procedure very similar to the ones used in AC2C and DC2C techniques can also be applied to the P2C model to obtain C_B as a function of the μ value of the balancing system. A target battery charge

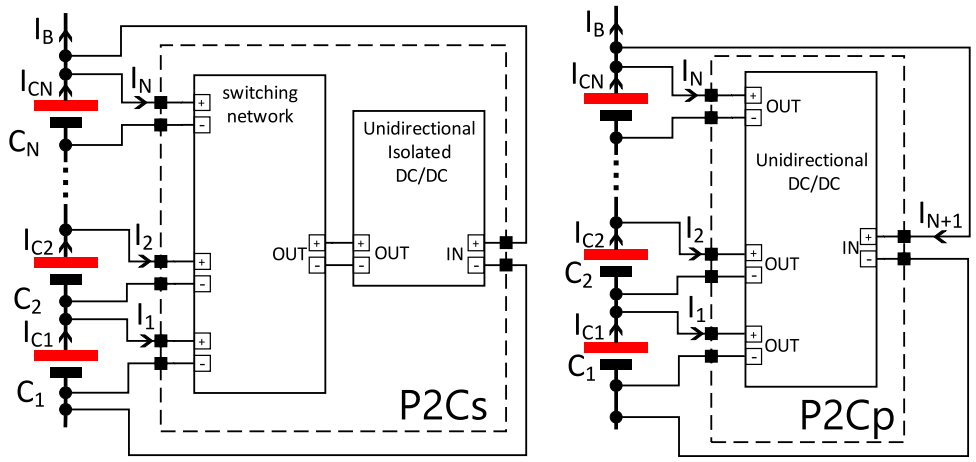

Fig. 10. Block diagram of a generic Pack-to-Cell active equalization system applied to a battery composed of N series-connected cells.

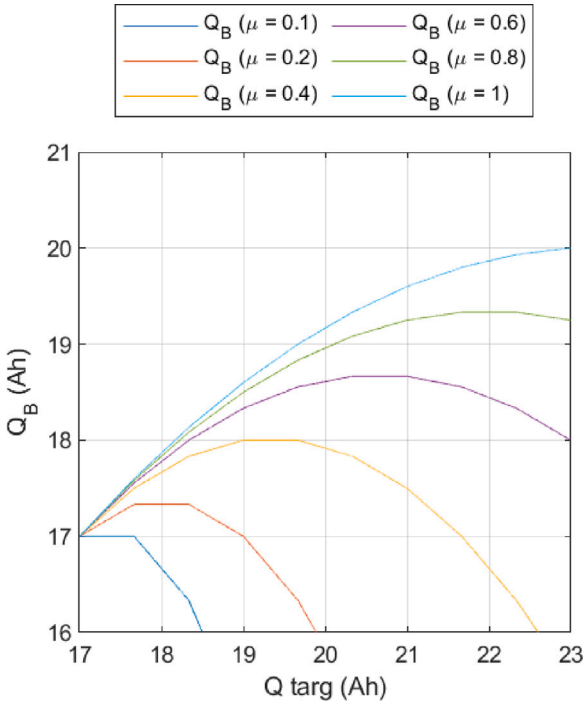

Fig. 11. Q_B values for Case A with different Q_{targ} and μ values.

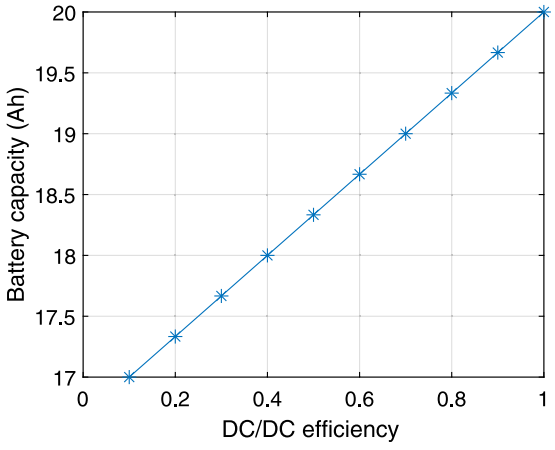

Fig. 12. C_B values obtainable with the Pack-to-Cell topology for different DC/DC efficiency μ with the cell capacity distribution of Case A.

value (Q_{targ}) is defined in the range from the minimum to the maximum cell capacity values. The quantity Q_j, equal to the difference between Q_{targ} and the cell capacity C_j, is calculated for each Q_{targ} value. The Q_j values represent the quantity of charge to add or remove from the cell j to reach an available quantity of charge equal to Q_{targ}. However, the unidirectional DC/DC converter only allows charge to be moved from the battery pack to the cells, so the positive values of Q_j must be set to 0. The sum of Q_j divided by $-\mu N$ is the quantity of charge that the DC/DC converter removes from all the battery cells, i.e. Q_{N+1}. The maximum quantity of charge that can be delivered from all the cells to the load (Q_B) is calculated using Eq. (15), which is obtained from the first equation group of the system (14) written with the charge variables.

$$Q_B = \min_{j\in[1,\dots,N]}(C_{C_j} - Q_{N+1} - Q_j) \tag{15}$$

Finally, C_B is the maximum value of Q_B that depends on Q_{targ}. This procedure is applied to Case A with μ in the range from 0.1 to 1. The value $\mu = 0$ is not considered, because the division between the sum of Q_j and μN leads to an illegal operation. The Q_B values obtained with Eq. (15) for each μ are reported in Fig. 11.

Fig. 11 shows that Q_B increases with Q_{targ} until the maximum value is reached. Then, if Q_{targ} increases Q_B starts to decrease because the contribution of the charge drained by the DC/DC converter from the battery pack is higher than the one delivered to the cells. The maximum values of each Q_B curve for a given μ is the value of C_B. These values are reported in Fig. 12 as a function of the converter transfer efficiency.

6. Cell-to-Pack (C2P)

The aim and the architecture of the C2P topology are very similar to those of P2C, as it can be noted from the block diagrams shown in Fig. 13. The only difference is that the DC/DC converters move energy from a given cell of the battery to the entire battery pack in this case. Two different architectures can also be defined for C2P topology: C2Ps, and C2Pp.

$$\begin{cases} I_{C_j} = I_B + I_{N+1} + I_j \quad \forall j = 1, \dots, N \\ I_j \geq 0 \quad \forall j = 1, \dots, N \\ I_{N+1} \leq 0 \\ -I_{N+1} = \frac{\mu}{N} \sum_{j=1}^{N} I_j \end{cases} \tag{16}$$

The model equations are reported in (16) and they are very similar to the P2C ones. However, the calculation of C_B is easier than in P2C

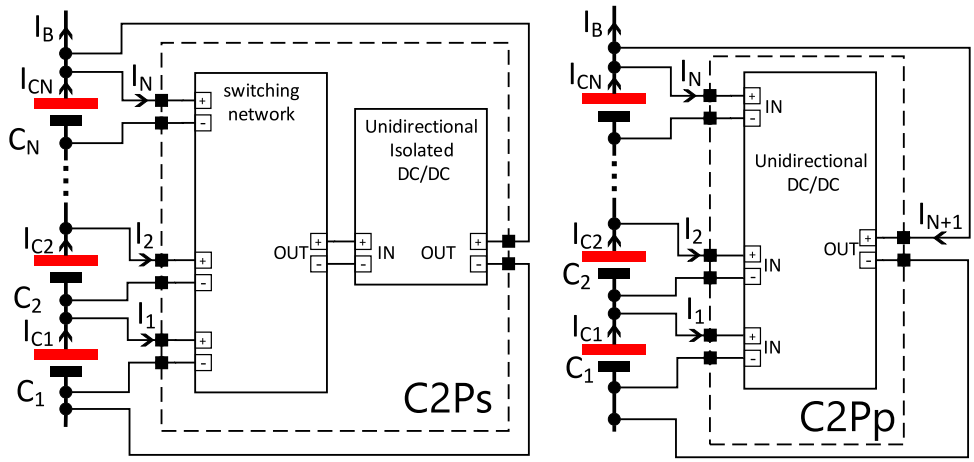

Fig. 13. Block diagrams of a generic Cell-to-Pack active equalization system applied to a battery composed of N series-connected cells.

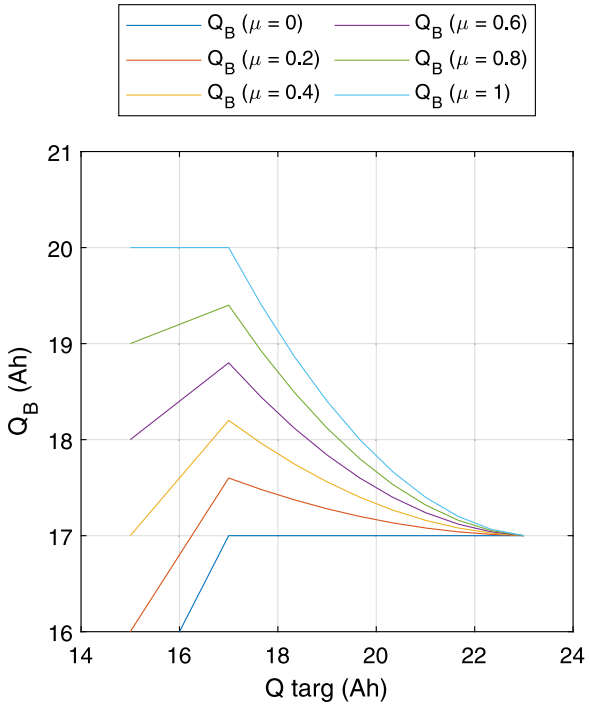

Fig. 14. Q_B values for Case A with different Q_{targ} and μ values.

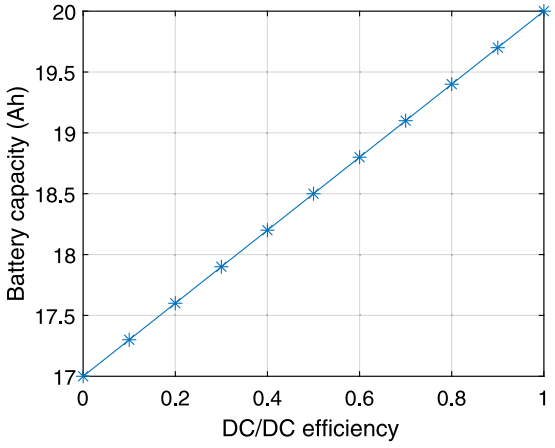

Fig. 15. C_B values obtainable with the Cell-to-Pack topology for different DC/DC efficiency μ with the cell capacity distribution of Case A.

topology because the unidirectional DC/DC converters move charge from single battery cells to the entire battery pack. The maximum capacity C_B is obtained by setting Q_{targ} equal to the minimum cell capacity. Indeed, each cell is discharged of a quantity of charge equal to $Q_{targ} - C_{C_j}$ in order to bring all the cell capacities equal to the minimum one. The process is very similar to passive balancing. However, the energy is not completely wasted as in passive balancing, because the extracted charge is returned to the pack and all the cells are charged with the same quantity of charge, thus maximizing the usable capacity of the battery. To better explain this concept, the same procedure explained for P2C topology is used with the C2P model to calculate the Q_B values for Case A with different Q_{targ} and μ values. The obtained Q_B values are reported in Fig. 14 in which we can note that the maximum Q_B value is obtained with Q_{targ} equal to the minimum cell capacity (85 % of 20 A h). Fig. 15 reports the maximum values of C_B obtained with different μ. These values are the maximum values of Q_B reported in Fig. 14.

7. Topology comparison

Let us now have a comparative evaluation of the different dynamic equalization techniques described in detail in the above sections.

7.1. Comparison of simulation results

The individual C_B curves for the AC2C, DC2C, P2C, and C2P topologies are shown in Fig. 16.

All the curves are obtained from case-study A except for topology AC2C. In this case, the same cell capacity distribution of Case A is used but all 10! permutations of the cell positions are considered since AC2C results strongly depend on the capacity mismatch distribution. The AC2C diagram reports the minimum and the maximum values of C_B as bottom and top of the error bars drawn over the relative mean value. The minimum value of C_B for AC2C is lower than in the other topologies for μ values higher than 0.1. On the other hand, the mean value of C_B is higher than those of the P2C and C2P topologies, whereas the maximum value is very similar to the one obtained with the DC2C topology. The DC2C topology shows the best performance in terms of usable capacity.

It is important to note that a significant quantity of charge is moved by the dynamic equalization circuit to obtain an improvement of the exploitable battery capacity. This quantity depends on the active balancing architecture adopted and the DC/DC converter efficiency. Fig. 17 shows and compares the quantity of charge moved with the

Table 1
Characteristics of some active balancing prototypes presented in literature.

	Architecture	Components					μ	I_{out}
		MOS	W	MC	C	D	(%)	(A)
AC2C	Buck–boost [36]	5n − 4,	n − 1				91	0.4
	Forward converter [37]	2n	2n − 1	n − 1			95	2
DC2C	LLC converter [38]	2n	2n	1	2n	2n	90	1
	Switched–Capacitor [39]	4n	2n		2n		95	0.4
	Flyback converter [40]	n	n/2	1			95	2.3
P2C	LCC converter [35]	2n + 2	4	1	1		88	0.5
	Forward–flyback [41]	n + 1	n + 1	1			84	0.7
C2P	Forward–flyback [41]	n + 1	n + 1	1			84	0.4

Note: n = number of cells, MOS = MOSfet, W = winding, MC = magnetic core, C = capacitor, D = Diode.

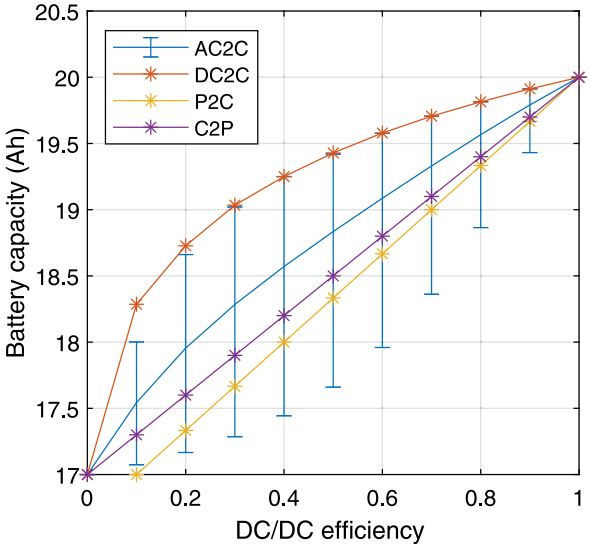

Fig. 16. Comparison of the battery capacity values obtainable with the presented topologies for different DC/DC efficiency μ values with the cell capacity distribution of Case A. All the possible permutations of the cell position are considered for the AC2C topology.

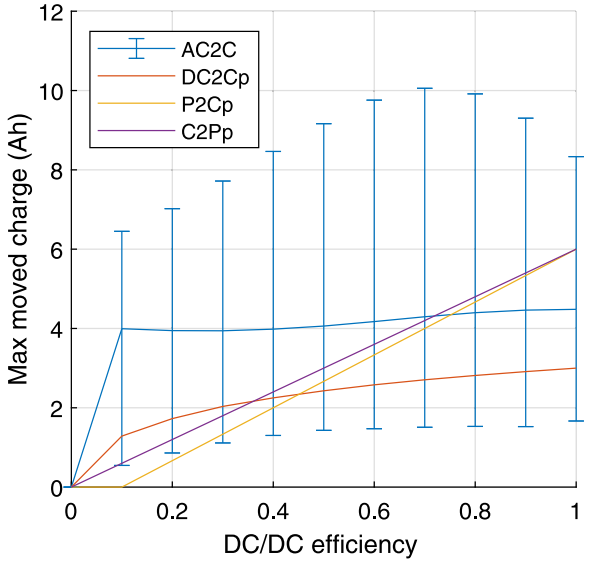

Fig. 17. Maximum charge moved by DC/DC converters in all the considered topologies for μ values in the range from 0 to 1.

AC2C, DC2Cp, P2Cp, and C2Pp topologies, as a function of DC/DC converter efficiency. The comparison is made by considering the charge passing through the output ports of the DC/DC converters for the various architectures. The maximum value of the charge for the AC2C, DC2Cp, and P2Cp topologies is considered. Instead, the value of the charge moved in the C2Pp topology is divided by the number of cells to obtain a fair comparison.

This comparison allows us to have an estimate of the power requested by the DC/DC converters to carry out the dynamic equalization. The higher is the moved quantity of charge, the higher is the DC/DC converter output current and power requested to perform a successful dynamic equalization. In other words, the architecture that moves a lower quantity of charge requires a lower power and less expensive DC/DC converters than the other architectures.

7.2. Application of state-of-the-art active balancing architectures to dynamic equalization

Let us now try to apply the simulation results obtained on the dynamic equalization topologies to a more realistic scenario. To this end, we considered the characteristics of some prototypes presented in the literature that were used as active balancing circuits [35–41]. These features are summarized in Table 1 that includes the main components, efficiency, and mean output current value I_{out} of the circuits.

The idea is to apply the reported circuits to a dynamic equalization scenario represented by our Case A and to compare them with respect to the cost, complexity, maximum achievable battery capacity C_B^*, and equalization time t_{Equ}. The comparison is shown in Table 2. The cost of each architecture is evaluated using the esteemed unit cost of each component provided in [42]. Instead, the architecture complexity is considered proportional to the number of MOSFETs in the circuit. The maximum achievable battery capacities are calculated by taking the simulation result shown in Fig. 16 that corresponds to the reported efficiency of the circuits. Finally, the equalization time t_{Equ} is obtained as the ratio between the maximum charge moved by the DC/DC converter shown in Fig. 17 and the reported current I_{out} of the investigated architecture.

The high efficiency of all the literature architectures allows them to reach very good performance in terms of achievable battery capacity. It is worth noting that the use of dynamic equalization leads to an increase from 14.5 to 17.4 % of the exploitable capacity of the battery. The DC2C flyback-based architecture presented in [40] has the best performances of cost, complexity, achievable battery capacity, and equalization time. However, the table highlights that the P2C and C2P topologies are suitable solutions to implement dynamic equalization thanks to their very good trade-off among cost, complexity, and efficiency.

The equalization time can be considered acceptable when compared to the time in which the battery is fully charged or discharged (t_a). The dynamic equalization system will not be able to maintain the SoC of all the battery cells balanced if t_{Equ} is higher than t_a. In this case, the usable battery capacity C_B becomes lower than C_B^* and the dynamic equalization technique fails to obtain the maximum achievable capacity

Table 2
Results of literature active balancing architecture applied to Case A second-life battery with dynamic equalization approach.

	Architecture	Cost ($)	Comp.	C_B^* (A h)	t_{Equ} (h)
AC2C	Buck–boost [36]	51.4	5	19.81	11.1
	Forward converter [37]	40.4	2	19.90	2.2
DC2C	LLC converter [38]	40	2	19.91	2.9
	Switched–Capacitor [39]	55	4	19.96	7.4
	Flyback converter [40]	14	1	19.96	1.3
P2C	LCC converter [35]	25.6	2	19.60	10.4
	Forward–flyback [41]	18.6	1	19.47	7.0
C2P	Forward–flyback [41]	18.6	1	19.52	12.6

Note: Cost per unit ($): MOS = 1, W = 0.6, MC = 1, C = 0.2, D = 0.15 [42].

gain. However, an improvement of the exploited battery capacity will always be obtained when dynamic equalization is used.

7.3. Comparison with the literature

The achievement of the above mentioned capacity gain makes dynamic equalization very appealing for second-life battery applications where the battery modules may be rather heterogeneous in performance.

The results obtained in this work confirm and extend those obtained in [18,22] in which the DC2C, P2C, and C2P topologies were compared one to the other and to the passive equalization circuit, in the scenario of charge balancing of the cells of a first-life battery. The authors only considered a SoC mismatch among the cells in that work, and the investigation of the possible cell capacity variation was not considered. Moreover, the figures of merit taken into account in [18,22] were the energy losses in the balancing process and the required balancing time. These performance indices are the most suited when the energy balance of the battery pack is required. On the contrary, the investigation reported in this paper is focused on the dynamic equalization technique that maximizes the usable capacity of a battery, one of the most important issues in second-life applications. In other words, the dynamic equalization methods investigated here are not performed once in a while when the cell charge mismatch in terms of SoC exceeds a given threshold. Instead, dynamic equalization is continuously applied to the battery, in order to extract the maximum possible charge during the operational tasks of the battery itself. Such capability is not needed in first-life applications, but it may become fundamental for the full exploitation of the battery performance in second-life applications, where the capacity mismatch of the cells may be relatively large.

8. Conclusions

This work has presented a novel methodology to study and compare the architectures for the active energy equalization among the cells of a battery . This methodology is applied to a second-life battery in which dynamic equalization allows cells with large capacity mismatch to be exploited at best. The proposed methodology is applied to compare the performance of Adjacent Cell-to-Cell, Direct Cell-to-Cell, Cell-to-Pack, and Pack-to-Cell active balancing topologies. The battery considered as case study has 10 series-connected cells with a capacity uniformly distributed in the range $20\,\text{A h} \pm 15\,\%$.

The comparison highlights that the Direct Cell-to-Cell architecture has the best performance among all the considered active balance topologies. Instead, the Adjacent Cell-to-Cell performance is strongly affected by the distribution of the mismatches among the cells in the battery. The results obtained by the simulation are combined with the characteristics of some active balancing circuits presented in the literature to verify the results in realistic scenarios. The considered active balancing circuits improve the exploited battery capacity when they are used in the dynamic equalization approach. The capacity obtained raises from 14.5 to 17.4 % with respect to the case in which no dynamic equalization is applied.

The results obtained show that the methodology described here can be useful to designers in the choice of the best architecture to implement the dynamic balancing approach for second-life battery applications, in order to mitigate the effects of the cell capacity mismatch and to facilitate the reuse of exhausted automotive batteries.

CRediT authorship contribution statement

Roberto Di Rienzo: Conceptualization, Methodology, Software, Validation, Investigation, Data curation, Writing – original draft, Visualization. **Niccolò Nicodemo:** Methodology, Validation, Resources, Writing – original draft. **Alessandro Verani:** Methodology, Validation, Resources, Writing – original draft. **Federico Baronti:** Software, Validation, Data curation, Writing – review & editing, Visualization. **Roberto Roncella:** Validation, Formal analysis, Writing – review & editing, Funding acquisition. **Roberto Saletti:** Conceptualization, Validation, Writing – original draft, Supervision, Project administration, Funding acquisition.

Declaration of competing interest

The authors declare that they have no known competing financial interests or personal relationships that could have appeared to influence the work reported in this paper.

Data availability

No data was used for the research described in the article.

Acknowledgments

This study was carried out within the MOST - Sustainable Mobility Center and received funding from the European Union NextGenerationEU (PIANO NAZIONALE DI RIPRESA E RESILIENZA (PNRR) - MISSIONE 4 COMPONENTE 2, INVESTIMENTO 1.4 - D.D. 1033 17/06/2022, CN00000023). Moreover, the project was partially funded under the National Recovery and Resilience Plan (NRRP), Mission 4 Component 2 Investment 1.3 - Call for tender No. 1561 of 11.10.2022 of Ministero dell'Universitá e della Ricerca (MUR); funded by the European Union - NextGenerationEU. The work was partially supported by the Ministero dell'Universitá e della Ricerca (MUR) in the framework of the FoReLab project (Departments of Excellence). This manuscript reflects only the authors' views and opinions, neither the European Union nor the European Commission can be considered responsible for them.

References

[1] J. Zhu, I. Mathews, D. Ren, W. Li, D. Cogswell, B. Xing, T. Sedlatschek, S.N.R. Kantareddy, M. Yi, T. Gao, Y. Xia, Q. Zhou, T. Wierzbicki, M.Z. Bazant, End-of-life or second-life options for retired electric vehicle batteries, Cell Rep. Phys. Sci. 2 (8) (2021) 100537, http://dx.doi.org/10.1016/j.xcrp.2021.100537.

[2] L. Maeyaert, L. Vandevelde, T. Doring, Battery storage for ancillary services in smart distribution grids, J. Energy Storage 30 (2020) 101524, http://dx.doi.org/10.1016/j.est.2020.101524.

[3] H. Sahebi, M. Khodoomi, M. Seif, M. Pishvaee, T. Hanne, The benefits of peer-to-peer renewable energy trading and battery storage backup for local grid, J. Energy Storage 63 (2023) 106970, http://dx.doi.org/10.1016/j.est.2023.106970.

[4] B. Gohla-Neudecker, M. Bowler, S. Mohr, Battery 2nd life: Leveraging the sustainability potential of EVs and renewable energy grid integration, in: 2015 International Conference on Clean Electrical Power, ICCEP, 2015, pp. 311–318, http://dx.doi.org/10.1109/ICCEP.2015.7177641.

[5] M. Einhorn, W. Roessler, J. Fleig, Improved performance of serially connected Li-ion batteries with active cell balancing in electric vehicles, IEEE Trans. Veh. Technol. 60 (6) (2011) 2448–2457, http://dx.doi.org/10.1109/TVT.2011.2153886.

[6] J. Carter, Z. Fan, J. Cao, Cell equalisation circuits: A review, J. Power Sources 448 (2020) 227489, http://dx.doi.org/10.1016/j.jpowsour.2019.227489.

[7] Y. Hua, S. Zhou, H. Cui, X. Liu, C. Zhang, X. Xu, H. Ling, S. Yang, A comprehensive review on inconsistency and equalization technology of lithium-ion battery for electric vehicles, Int. J. Energy Res. 44 (14) (2020) 11059–11087, http://dx.doi.org/10.1002/er.5683.

[8] A. Turksoy, A. Teke, A. Alkaya, A comprehensive overview of the DC-DC converter-based battery charge balancing methods in electric vehicles, Renew. Sustain. Energy Rev. 133 (2020) 110274, http://dx.doi.org/10.1016/j.rser.2020.110274.

[9] R. Di Rienzo, M. Zeni, F. Baronti, R. Roncella, R. Saletti, Passive balancing algorithm for charge equalization of series connected battery cells, in: 2020 2nd IEEE International Conference on Industrial Electronics for Sustainable Energy Systems, Vol. 1, IESES, 2020, pp. 73–79, http://dx.doi.org/10.1109/IESES45645.2020.9210643.

[10] T. Baumhofer, M. Bruhl, S. Rothgang, D.U. Sauer, Production caused variation in capacity aging trend and correlation to initial cell performance, J. Power Sources 247 (2014) 332–338, http://dx.doi.org/10.1016/j.jpowsour.2013.08.108.

[11] N. Kutkut, D. Divan, Dynamic equalization techniques for series battery stacks, in: Proceedings of Intelec'96 - International Telecommunications Energy Conference, 1996, pp. 514–521, http://dx.doi.org/10.1109/INTLEC.1996.573384.

[12] N.S. Mubenga, K. Sharma, T. Stuart, A bilevel equalizer to boost the capacity of second life Li-ion batteries, Batteries 5 (3) (2019) http://dx.doi.org/10.3390/batteries5030055.

[13] Z. Ma, F. Gao, X. Gu, N. Li, Q. Wu, X. Wang, X. Wang, Multilayer SOH equalization scheme for MMC battery energy storage system, IEEE Trans. Power Electron. 35 (12) (2020) 13514–13527, http://dx.doi.org/10.1109/TPEL.2020.2991879.

[14] D. Oeser, A. Ziegler, B. Arndt, A. Ackva, Effectiveness of active balancing on high dispersion batteries, in: 2018 International IEEE Conference and Workshop in Obuda on Electrical and Power Engineering (CANDO-EPE), 2018, pp. 21–26, http://dx.doi.org/10.1109/CANDO-EPE.2018.8601129.

[15] A. Devie, G. Baure, M. Dubarry, Intrinsic variability in the degradation of a batch of commercial 18650 lithium-ion cells, Energies 11 (5) (2018) http://dx.doi.org/10.3390/en11051031.

[16] Y. Hua, S. Zhou, Y. Huang, X. Liu, H. Ling, X. Zhou, C. Zhang, S. Yang, Sustainable value chain of retired lithium-ion batteries for electric vehicles, J. Power Sources 478 (2020) 228753, http://dx.doi.org/10.1016/j.jpowsour.2020.228753.

[17] M. Einhorn, W. Guertlschmid, T. Blochberger, R. Kumpusch, R. Permann, F.V. Conte, C. Kral, J. Fleig, A current equalization method for serially connected battery cells using a single power converter for each cell, IEEE Trans. Veh. Technol. 60 (9) (2011) 4227–4237, http://dx.doi.org/10.1109/TVT.2011.2168988.

[18] F. Qu, Q. Luo, H. Liang, D. Mou, P. Sun, X. Du, Systematic overview of active battery equalization structures: Mathematical modeling and performance evaluation, IEEE Trans. Energy Convers. 37 (3) (2022) 1685–1703, http://dx.doi.org/10.1109/TEC.2022.3142818.

[19] M. Caspar, T. Eiler, S. Hohmann, Systematic comparison of active balancing: A model-based quantitative analysis, IEEE Trans. Veh. Technol. 67 (2) (2018) 920–934, http://dx.doi.org/10.1109/TVT.2016.2633499.

[20] Y.-X. Wang, H. Zhong, J. Li, W. Zhang, Adaptive estimation-based hierarchical model predictive control methodology for battery active equalization topologies: Part I Balancing strategy, J. Energy Storage 45 (2022) 103235, http://dx.doi.org/10.1016/j.est.2021.103235.

[21] Y.-X. Wang, H. Zhong, J. Li, W. Zhang, Adaptive estimation-based hierarchical model predictive control methodology for battery active equalization topologies: Part II - equalizer control, J. Energy Storage 45 (2022) 102958, http://dx.doi.org/10.1016/j.est.2021.102958.

[22] F. Baronti, R. Roncella, R. Saletti, Performance comparison of active balancing techniques for lithium-ion batteries, J. Power Sources 267 (2014) 603–609, http://dx.doi.org/10.1016/j.jpowsour.2014.05.007.

[23] Z. Zhao, H. Hu, Z. He, H.H.-C. Iu, P. Davari, F. Blaabjerg, Power electronics-based safety enhancement technologies for lithium-ion batteries: An overview from battery management perspective, IEEE Trans. Power Electron. 38 (7) (2023) 8922–8955, http://dx.doi.org/10.1109/TPEL.2023.3265278.

[24] N. Ghaeminezhad, Q. Ouyang, X. Hu, G. Xu, Z. Wang, Active cell equalization topologies analysis for battery packs: A systematic review, IEEE Trans. Power Electron. 36 (8) (2021) 9119–9135, http://dx.doi.org/10.1109/TPEL.2021.3052163.

[25] P. Soni, I. Karuppasamy, Performance analysis of a 48V battery pack using SoC estimation and cell balancing for electric vehicle, in: 2023 IEEE 8th International Conference for Convergence in Technology (I2CT), 2023, pp. 1–6, http://dx.doi.org/10.1109/I2CT57861.2023.10126257.

[26] L. Barzacchi, M. Lagnoni, R.D. Rienzo, A. Bertei, F. Baronti, Enabling early detection of lithium-ion battery degradation by linking electrochemical properties to equivalent circuit model parameters, J. Energy Storage 50 (2022) 104213, http://dx.doi.org/10.1016/j.est.2022.104213.

[27] R. Morello, R. Di Rienzo, R. Roncella, R. Saletti, F. Baronti, Hardware-in-the-loop platform for assessing battery state estimators in electric vehicles, IEEE Access 6 (2018) 68210–68220, http://dx.doi.org/10.1109/ACCESS.2018.2879785.

[28] W. Zhang, L. Wang, L. Wang, C. Liao, Y. Zhang, Joint state-of-charge and state-of-available-power estimation based on the online parameter identification of lithium-ion battery model, IEEE Trans. Ind. Electron. 69 (4) (2022) 3677–3688, http://dx.doi.org/10.1109/TIE.2021.3073359.

[29] S. Xu, K. Gao, X. Zhang, K. Li, Double-layer e-structure equalization circuit for series connected battery strings, Energies 12 (22) (2019) http://dx.doi.org/10.3390/en12224252.

[30] E. Ekanayake, K. Hemapala, U. Jayathunga, Active and passive based hybrid cell balancing approach to series connected lithium-ion battery pack, in: 2022 Moratuwa Engineering Research Conference (MERCon), 2022, pp. 1–6, http://dx.doi.org/10.1109/MERCon55799.2022.9906172.

[31] R. de Castro, C. Pinto, J. Varela Barreras, R.E. Araújo, D.A. Howey, Smart and hybrid balancing system: Design, modeling, and experimental demonstration, IEEE Trans. Veh. Technol. 68 (12) (2019) 11449–11461, http://dx.doi.org/10.1109/TVT.2019.2929653.

[32] S.K. Dam, V. John, Low-frequency selection switch based cell-to-cell battery voltage equalizer with reduced switch count, IEEE Trans. Ind. Appl. 57 (4) (2021) 3842–3851, http://dx.doi.org/10.1109/TIA.2021.3075184.

[33] F. Baronti, R. Di Rienzo, R. Moras, R. Roncella, R. Saletti, G. Pede, F. Vellucci, Implementation of the fast charging concept for electric local public transport: The case-study of a minibus, in: 2015 IEEE 13th International Conference on Industrial Informatics, INDIN, 2015, pp. 1284–1289, http://dx.doi.org/10.1109/INDIN.2015.7281920.

[34] R. Di Rienzo, F. Baronti, F. Vellucci, F. Cignini, F. Ortenzi, G. Pede, R. Roncella, R. Saletti, Experimental analysis of an electric minibus with small battery and fast charge policy, in: 2016 International Conference on Electrical Systems for Aircraft, Railway, Ship Propulsion and Road Vehicles & International Transportation Electrification Conference (ESARS-ITEC), 2016, pp. 1–6, http://dx.doi.org/10.1109/ESARS-ITEC.2016.7841433.

[35] Z. Wei, F. Peng, H. Wang, An LCC-based string-to-cell battery equalizer with simplified constant current control, IEEE Trans. Power Electron. 37 (2) (2022) 1816–1827, http://dx.doi.org/10.1109/TPEL.2021.3102627.

[36] S. Wang, S. Yang, W. Yang, Y. Wang, A new kind of balancing circuit with multiple equalization modes for serially connected battery pack, IEEE Trans. Ind. Electron. 68 (3) (2021) 2142–2150, http://dx.doi.org/10.1109/TIE.2020.2973886.

[37] T.H. Phung, A. Collet, J.-C. Crebier, An optimized topology for next-to-next balancing of series-connected lithium-ion cells, IEEE Trans. Power Electron. 29 (9) (2014) 4603–4613, http://dx.doi.org/10.1109/TPEL.2013.2284797.

[38] R. Zou, F. Liu, Y. Liu, G. Xu, F. Liu, An LLC-based battery equalizer with inherent current limitation, IEEE Trans. Power Electron. 37 (2) (2022) 1828–1840, http://dx.doi.org/10.1109/TPEL.2021.3103534.

[39] L. Liu, R. Mai, B. Xu, W. Sun, W. Zhou, Z. He, Design of parallel resonant switched-capacitor equalizer for series-connected battery strings, IEEE Trans. Power Electron. 36 (8) (2021) 9160–9169, http://dx.doi.org/10.1109/TPEL.2021.3052780.

[40] Y. Shang, N. Cui, C. Zhang, An optimized any-cell-to-any-cell equalizer based on coupled half-bridge converters for series-connected battery strings, IEEE Trans. Power Electron. 34 (9) (2019) 8831–8841, http://dx.doi.org/10.1109/TPEL.2018.2888514.

[41] Y. Li, J. Xu, X. Mei, J. Wang, A unitized multiwinding transformer-based equalization method for series-connected battery strings, IEEE Trans. Power Electron. 34 (12) (2019) 11981–11989, http://dx.doi.org/10.1109/TPEL.2019.2910205.

[42] A.M. Imtiaz, F.H. Khan, Time shared flyback converter based regenerative cell balancing technique for series connected li-ion battery strings, IEEE Trans. Power Electron. 28 (12) (2013) 5960–5975, http://dx.doi.org/10.1109/TPEL.2013.2257861.